Planetary and Space Science 59 (2011) 1069–1081

Contents lists available at ScienceDirect

Planetary and Space Science

journal homepage: www.elsevier.com/locate/pss

Revealing Mars' deep interior: Future geodesy missions using radio links between landers, orbiters, and the Earth

V. Dehant [a,*], S. Le Maistre [a], A. Rivoldini [a], M. Yseboodt [a], P. Rosenblatt [a], T. Van Hoolst [a], M. Mitrovic [a], Ö. Karatekin [a], J.C. Marty [b], A. Chicarro [c]

[a] Royal Observatory of Belgium, Av. Circulaire 3, B-1180 Brussels, Belgium
[b] Centre National d'Etudes Spatiales (CNES), Toulouse et Groupe de Recherche en Géodésie Spatial (GRGS), France
[c] ESTEC/ESA, The Netherlands

ARTICLE INFO

Article history:
Received 20 October 2009
Received in revised form
15 March 2010
Accepted 18 March 2010
Available online 9 April 2010

Keywords:
Geodesy
Nutation
Mars interior
Mars core

ABSTRACT

In the frame of a comparison between Earth, Venus, and Mars, a vision on future geodesy missions to Mars is discussed with particular focus on furthering our understanding of the interior, rotation, and orientation of this terrestrial planet. We explain how radioscience instruments can be used to observe the rotation and orientation and therewith to study the deep interior of Mars and its global atmosphere dynamics. Transponders in X-band and Ka-band are proposed with radio links between a lander or a rover and an orbiter around Mars and/or directly to the Earth. The radio budget links are studied in the frame of possible mission constraints and simulations are performed, which show that important information on the interior of Mars can be obtained from the radioscience data. From the observation of Mars' orientation in space and of tidal effects on a spacecraft orbiting around Mars we show that it is possible for instance to constrain the dimension and composition of the core, the percentage of light element within the core, and to determine the presence of a pressure-induced mineral-phase transition at the bottom of the mantle.

1. Physical phenomena observed in radioscience

The objectives of radioscience missions are numerous (see e.g. Barriot et al., 2001; Konopliv et al., 2006, in press; Zuber et al., 2007; Pätzold et al., 2009; 2010) and go from detailed studies of Mars' atmosphere (neutral atmosphere and ionosphere), the determination and analysis of its global mass repartition, the study of the surface properties such as roughness, the study of the subsurface mass repartition, the study of the interior of Mars, to Mars' ephemerides. These objectives are reached either by analyzing the Doppler or ranging signal directly reaching the Earth from the spacecraft, or by performing occultations and reflections from surfaces (bi-static radar) analyses of the radio signals. The study of Mars may even be complemented with study of the solar corona from radioscience. In this paper, we will concentrate on the study of Mars' interior and atmospheric global dynamics as determined from Mars' orientation and rotation parameters and from time variations of the gravity field as determined from spacecraft tracking. Lander–Earth or lander–orbiter radio links allow observing Mars' rotation rate variations (or length-of-day (LOD) variations, arising from the effect of the CO_2 sublimation and condensation processes), Mars' polar motion (also excited by the atmosphere), and Mars' orientation in space, i.e. precession/nutation (arising from the gravitational interactions between Mars and the Sun or the other planets of the solar system). Precession and nutations provide fundamental constraints on the properties of Mars' deep interior such as core state, composition, and dimension (Dehant et al., 2000a, 2000b; Van Hoolst et al., 2000a; Van Hoolst, 2007), while rotation variations or LOD variations provide atmospheric angular momentum changes that are measures of the global dynamics of Mars' atmosphere (Defraigne et al., 2000; Van den Acker et al., 2002; Karatekin et al., 2006b). In particular the LOD seasonal variations are related to the CO_2 sublimation and condensation cycle in the ice caps and atmosphere. The nutations, i.e. the periodic changes in the orientation of the planet in space, are very interesting as they are amplified when the core is liquid. Different dimensions for the core induce different amplifications. The nutations, if observed with enough precision (at a level of better than a few milliarcseconds (*mas*)), will provide an independent observation of the state of the core and allow to

* Corresponding author.
E-mail addresses: v.dehant@oma.be (V. Dehant), sebastien.maitre@oma.be (S. Le Maistre), rivoldini@oma.be (A. Rivoldini), yseboodt@oma.be (M. Yseboodt), rosenblatt@oma.be (P. Rosenblatt), tim.vanhoolst@oma.be (T. Van Hoolst), mitrovic@oma.be (M. Mitrovic), karatekin@oma.be (Ö. Karatekin), jean-charles.marty@cnes.fr (J.C. Marty), Agustin.Chicarro@esa.int (A. Chicarro).

0032-0633/$ - see front matter © 2010 Elsevier Ltd. All rights reserved.
doi:10.1016/j.pss.2010.03.014

estimate its size; the formation and evolution of Mars will better be constrained. In particular, the resonance period and amplification of the free core nutation (FCN), a rotational normal mode of the planet due to the existence of a liquid ellipsoidal core, depend on the dimension of the core and on the core moment of inertia. This FCN period is close to the ter-annual nutation (229 days) (see Dehant et al., 2000a, 2000b; Van Hoolst et al., 2000a, 2000b; Defraigne et al., 2003; Van Hoolst, 2007); it may be very close if the core is large (FCN period close to 235 days for instance), amplifying this nutation at a very high level, and it may be quite far if the core is small (FCN period close to 263 days for instance). This amplification may thus reach values between almost no amplification (sub-*mas* level; 0.9 mas for instance for a 263 day FCN period) and amplification at the 100% level (10 *mas* level for instance for a 235 day FCN period) or several hundreds of percents (when the FCN is very close to the 229 days of the ter-annual nutation period; e.g. 27 mas for 231 day FCN period); this amplification is quite high as 1 *mas* corresponds to 1.6 cm at the surface of Mars when considering the displacement of the pole in space. Lander links may also be used to study the periodic soil deformations induced by the tides (see Dehant et al., 2000a; Van Hoolst et al., 2003) or by the seasonal atmospheric loading (Karatekin et al., 2006a; Métivier et al., 2008). If precise enough (sub-cm level), the displacements of the surface may also provide information about the interior of Mars such as core dimension and light element concentration and complement our understanding of the thermal state and evolution of the planet.

Orbiter–Earth radio links can also provide information about the tides and therewith about the deep interior of Mars. The periodic deformations of Mars induced by the gravitational forcing of the Sun and the other planets of the solar system induce changes in the spacecraft orbit dynamics: the change in the gravity field induced by the planet tides is mapped into the orbiter trajectory. This effect is measured through the Love number k_2, i.e. the ratio between the mass redistribution potential induced by the tides to the tidal potential. The value of k_2 depends very much on the interior of Mars and, in particular, if the core is liquid, the planet deforms more in response to the tidal forcing, increasing the value of the Love number k_2. The value of k_2 for a solid core ($k_2 \sim 0.07$) is at the level of about one half of that for a liquid core ($k_2 \sim 0.15$). The precision on the k_2 Love number depends on the precision of the orbit determination. It is however difficult to precisely provide numbers in this case, as it is important to consider the geometry of the orbit of the orbiter; particular orbits are better than others for determining the tidal effects.

From recent radioscience observations of the k_2 tidal Love number, we have good indications that the core is at least partially liquid, which is compatible with the present day thinking of the evolution models of Mars. Mars interior models have been built by Sohl and Spohn in 1997 (and later on by Bertka and Fei, 1998; Sanloup et al., 1999; Zharkov and Gudkova, 2000) based on knowledge inferred from the SNC meteorites and/or accounting for the moment of inertia derived from radioscience precession observation (Folkner et al., 1997). Presently, the best information about the core is deduced from the effect of Mars tides on the trajectory of an orbiter by tracking the effects of Mars' tides on the trajectory of an orbiter (from the determination of the tidal Love number k_2) and from the precession of the spin axis derived from radiotracking of orbiting and landed spacecraft (e.g., Smith et al., 1998; Folkner et al., 1997; Yoder et al., 2003; Konopliv et al., 2006; Balmino et al., 2006; Marty et al., 2009).

The presence or not of an inner core is presently determined indirectly from the absence of a global magnetic field and from geochemical and thermal conditions in the core. From the thermal and mineralogical possibilities for Mars, only relatively small cores with a small percentage of light elements would provide the possibility to have a solid inner core inside Mars. As it will be seen later in the paper, the present-day range of values of the tidal Love number would marginally allow the presence of a solid inner core (when the k_2 values would be very small).

Radioscience can in addition be jointly used with other instruments foreseen in network science like seismometers, magnetometers, and heat flow measuring devices (see Harri et al., 1999; Lognonné et al., 1999; Dehant et al., 2004; Grott et al., 2007; Mocquet et al., 2010). This is particularly true for the objective of obtaining information on the interior of the planet Mars such as physical state, composition, density, and temperature profiles (see Verhoeven et al., 2005) as data from seismometers, magnetometers, and transponders may be jointly used to deduce the profiles of temperature and mineralogy of Mars. Heat flow measurements will also help in our understanding of these properties of the interior of Mars.

The question of the existence of a solid inner core within the liquid core may be addressed as well, not only using future seismic observations, but also possibly using radioscience. The presence of an inner core depends on the core constituents and on the temperature at the core-mantle boundary. Observing a signature of the inner core is thus a very important constraint on the models of Mars' interior. However, a small inner core would only induce influences on the nutation below 1 mas (milliarcsecond) (Van Hoolst et al., 2000a; Defraigne et al., 2003; Dehant et al., 2003). As also detailed in Van Hoolst (2007) the inner core and its moment of inertia are too small to noticeably influence the FCN, which is essentially a differential rotation of the outer core, and to induce a non-negligible effect of the free inner core nutation (FICN) on nutations (the FICN is a rotational normal mode of the planet due to the existence of an ellipsoidal solid inner core in the liquid core, when there is an inner core inside Mars). For decrease in light-element concentration in the liquid core, and increase in inner core radius, this situation may change: a large inner core could have a measurable effect on the nutations as for instance the amplification due to the FCN resonance on the prograde semi-annual nutation is almost canceled by the resonance to the FICN (see e.g. Defraigne et al., 2003). Failure to detect the liquid core amplification of the semi-annual prograde nutation could then be interpreted as evidence for a large inner core. Again, this requires a sufficiently accurate geodesy experiment (at better than a few mas level).

Similarly the effects of a possible inner core on the Love number k_2 as determined from orbiter radioscience depend on the dimension of the inner core and will be hard to determine. As already mentioned the precision on the k_2 determination depends as well on the geometry of the orbit and the tracking strategy.

Similar conclusions hold for the time variations of the gravity field induced by the CO_2 sublimation and condensation process, as discussed in Karatekin et al. (2005a). In particular, the inclination and eccentricity of the orbit as well as the geometry of the orbiter-to-Earth line-of-sight (edge-on or face-on observations) change the contribution of time-variable gravity to the Doppler.

2. Measurement types in radioscience and present-day knowledge

In order to assess the possibility to obtain information on the interior of Mars, we have built models of the interior of Mars and computed the geophysical parameters that will be measured from radioscience experiments. We have then used these parameters in order to simulate the contributions to Doppler and ranging measurements. For a mineralogy often used in these kinds of simulations, the Dreibus and Wänke (1985) mineralogy, we have

built (as detailed in Rivoldini et al., 2010) interior models in agreement with the observed range of k_2 values (in the interval [0.117, 0.157]) and with the moment of inertia (0.365 for the scaled moment of inertia) deduced from geodetic observations, respectively, the tidal contributions on the time variable gravity acting on a spacecraft as measured by radioscience and the precession observed from landers at the surface of Mars (see Folkner et al., 1997) and orbiters (see Konopliv et al., 2006). In these models, we have allowed for a range of light element concentrations in the core (below 20 wt%), a range of density in the crust (between 2750 and 3000 kg/m^3) and of crustal thicknesses (between 60 and 90 km). For a variety of reasons, sulfur is thought to be the main light element that in the very early stages of the evolution of Mars descends with iron in the planet to form the Martian core (Dreibus and Wänke, 1987; Sohl and Spohn, 1997; Rivoldini et al., 2009). The density and elastic properties as a function of depth have been calculated as a function of local pressure and temperature by using equations of state, phase diagrams, and recent data about thermoelastic properties of mantle mineralogy phases and core constituents (see Rivoldini et al., 2010). These models turn out to be in favor of a molten core, a core size of about 1640 ± 150 km, a sulfur weight fraction of 12.8 ± 6.0 wt%, and the bulk of the models have temperature and pressure conditions in the lowest part of the mantle suitable for the phase transition to the mineral phase perovskite to occur. This endogenic phase transition may help sustaining large long-standing plumes possibly responsible for the Tharsis rise (Breuer et al., 1997; Spohn et al., 2001; Van Thienen et al., 2006, 2007). The relatively large uncertainties on the core size and core sulfur concentration result from the large range of possible k_2 values that have been deduced from different radioscience teams using the same radioscience data (Konopliv et al., 2006; Marty et al., 2009). These two recent estimates of the Love number k_2 are: $k_2 = 0.148 \pm 0.009$ (Konopliv et al., 2006, solution from MGS and Odyssey spacecraft (0.156), corrected for the effects of the thermal tide in the atmosphere and for the mantle anelasticity, i.e. -0.008) and $k_2 = 0.120 \pm 0.003$ (Marty et al., 2009). Konopliv et al. (2006) have found differences between the Love number solutions of the MGS and Odyssey spacecraft (either alone or combined), which they attributed partly to unmodeled atmospheric solar tide effects and to unmodeled spacecraft forces for Odyssey. The value of Konopliv et al. has been corrected for the effects of the thermal tide in the atmosphere and for the mantle anelasticity while the value of Marty et al. has not. We use these values as a first step in our sensitivity evaluation. They may change in the future by considering new radioscience and spacecraft data, applying solar atmospheric corrections to the values, and accounting for the mantle inelasticity.

Besides tidal potential variations and spin axis precession, also the nutations are sensitive to the interior structure of a planet. The nutations, being the response of Mars to the gravitational forcing of the Sun (and to a minor extent of Phobos and Deimos and of the other planets of the solar system), are amplified if the core is liquid because of a resonance with the free core nutation (FCN) rotational normal mode of Mars. The nutations are thus sensitive to the core physical state and to the dimension of the core through the FCN resonance. The resonance does not exist if the core is solid. For a liquid or partially liquid core, the amplification of the nutation depends on the period of the FCN normal mode, which depends (among others) on the core dimension (see Dehant et al., 2000a, 2000b; Van Hoolst et al., 2000a, 2000b; Van Hoolst, 2007; Defraigne et al., 2003; Dehant et al., 2003). The closer the nutation frequency is to the FCN frequency, the larger the amplification.

Fig. 1 shows the FCN period as a function of the core radius computed for the interior models that are within the range of

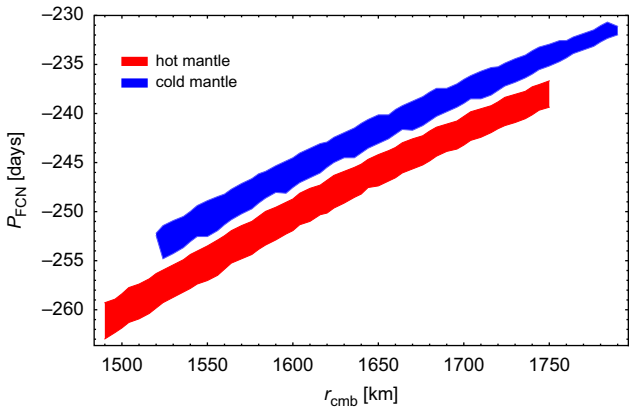

Fig. 1. FCN period as a function of core size for hot and cold mantle temperature end-members and the Dreibus–Wänke mantle mineralogy. The range in core size corresponds to those models that are compatible with the k_2 values of Konopliv et al. (2006) and Marty et al. (2009).

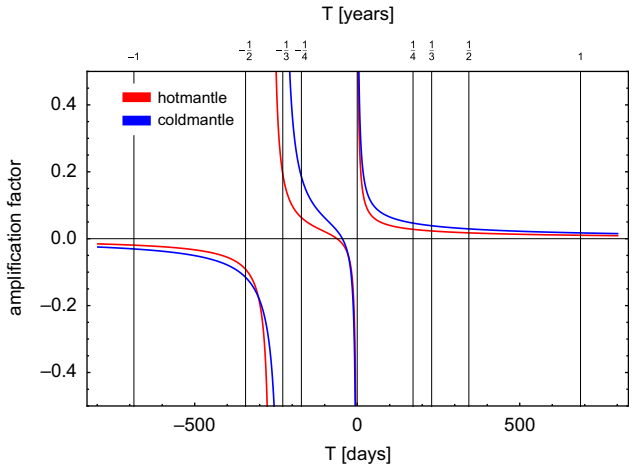

Fig. 2. Liquid core resonance effects on the nutation transfer function (liquid core amplification factor) for different core dimensions and the mantle mineralogy of Dreibus and Wänke (1985), as a function of the period T in days. Blue (for large core) and red (for smaller core) denote the limits obtained from the different extreme values of the tidal k_2 Love number observed from spacecraft by Konopliv et al. (2006) and Marty et al. (2009). The vertical lines indicate the Martian nutation frequencies. (For interpretation of the references to colour in this figure legend, the reader is referred to the web version of this article.)

possible k_2 values considered in this paper and with the modeling constraints explained above. The 'thickness' of each of the two 'curves' is related to the different possibilities in the models (e.g. changes in the crustal density and thickness); the two 'curves' correspond to the two end-members of possible temperature profiles for the mantle (cold or hot mantle). The figure shows that an observational determination of the FCN period can be used to constrain the core radius. Observations of the FCN resonance amplification (and frequency) in the nutations will therefore constrain the size of the Martian core. This is illustrated in Fig. 2, which shows the computed nutation contribution scaled by the forcing, i.e. the so-called transfer function, as a function of the period T for two end-member models (with the mantle mineralogy of Dreibus and Wänke (1985) and constrained by the tidal k_2 Love number considering in the range explained above) corresponding to the extreme values of the FCN periods of Fig. 1. The two end-member models are characterized by the properties provided in Table 1. The resonance with the FCN is clearly visible in Fig. 2; its location

Table 1
Properties of the two end-members models of the interior of Mars.

Models	Radius of the CMB (km)	Crust thickness (km)	Crust density (kg/m^3)	Core sulfur concentration (wt%)	Temperature of the mantle	k_2	Moment of inertia	FCN [days]
mod1	1490	60	3000	7	Hot	0.117	0.3647	−263.0
mod2	1790	90	2750	19	Cold	0.157	0.3658	−231.1

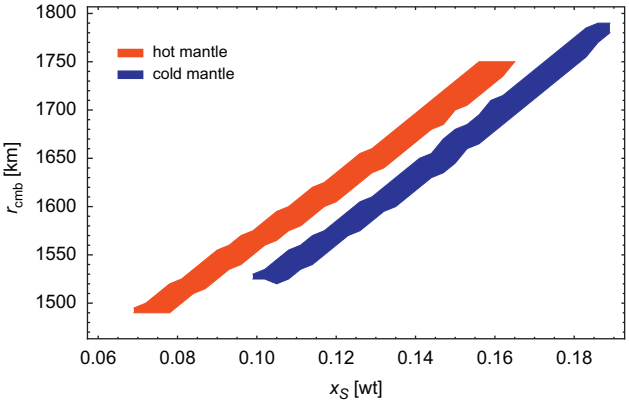

Fig. 3. Core size and core mantle boundary pressure as a function of core sulfur concentration for hot and cold mantle temperature end-members and the Dreibus–Wänke mantle mineralogy for Mars interior structure models that are compatible with the k_2 values of Konopliv et al. (2006) and Marty et al. (2009).

depends on the FCN period and thus on the size of the core. The vertical lines indicate the Martian nutation frequencies, i.e. the frequencies at which nutations can be observed. One can see that the retrograde ter-annual nutation gets amplified very differently for the different models. The ter-annual nutation experiences a significantly stronger amplification for the model with the larger the core size since the FCN period decreases toward the ter-annual period with increasing core size. Observing this nutation will thus significantly increase our knowledge and our understanding of Mars' interior. As a further example of this, Fig. 3 shows that a better constraint on the core size also implies a better knowledge of the light element concentration in the core.

3. Lander–Earth simulations and information on Mars' interior

Simulations (see Dehant et al., 2009; Le Maistre et al., submitted for publication) have shown that it is possible to detect the nutation signature on Doppler measurements performed with a lander, and therewith to obtain the state (solid or liquid or both) and size of the core. Fig. 4 shows, as a function of the mission duration, the solutions obtained for the main prograde and retrograde nutation amplitudes from numerical simulations done with the Géodésie par Intégrations Numériques Simultanées (GINS) software developed by CNES and further adapted at ROB for planetary geodesy applications. The computations have been done by simulating an X-band radio link between an equatorial lander and the Earth when the Earth is between 20° and 40° in the lander sky and for 45 min of Doppler tracking twice a week. The FCN considered in this simulation had a period of 240 days and core radius is 1650 km. The figure shows the true error and the formal error; the first one consists of the difference between the true value of the parameter used to simulate the data and its estimated value after processing of the simulated data (with noise); the formal error is the square root of the posteriori variance that comes from the least square analysis. The horizontal dotted lines indicate the level above which we expect to have information on the interior of Mars (with respect to our present knowledge coming from theory). The errors on the nutation amplitudes should therefore be below these lines in order to bring information on Mars' deep interior. The figure shows that mainly the retrograde ter-annual nutation (response to the ter-annual forcing of the Sun on Mars) will allow providing the core dimension. The prograde semi-annual nutation will only allow confirmation of the presence of a liquid core and possibly detecting an inner core. The core dimension considered in this simulation is a nominal value; a larger core would show larger amplifications of the ter-annual nutation and of the semi-annual nutation (Rivoldini et al., 2010); typical numbers for these amplifications are 1 mas and 9 mas for the retrograde ter-annual and prograde semi-annual nutations, respectively, for a small core of about 1490 km and 27 mas and 15 mas for the retrograde ter-annual and prograde semi-annual nutations, respectively, for a large core of about 1790 km (see Rivoldini et al., 2010, for discussions).

It must be mentioned that very recently the tidal Love number has been re-determined from the perturbations of the orbits of Mars Global Surveyor (MGS) and Mars Odyssey observed from most recent radiotracking of these spacecraft (Konopliv et al., in press). The large k_2 Love number value (0.159, after the thermal atmospheric tides and mantle anelasticity corrections) suggests an even larger core that is completely liquid. Such a large core would induce an FCN even closer to the retrograde ter-annual nutation and a higher amplification of this last nutation. The detection of the signature on the nutation will undoubtfully be feasible with an X-band direct radiolink from the surface of the planet Mars to the Earth ground station.

4. Future radiolink opportunities for radioscience

In the previous section we have shown the potential of bringing information on Mars deep interior from radioscience observation of nutations and tidal effects. In this section we discuss the future possibilities for realizing these observations and the requested accuracy of the instruments used. Generally speaking, future radioscience experiments will use radio links at different frequency bands, mainly X-, Ka-, and UHF links (see Tables 2 and 3), abandoning the S-band previously used as in the Viking missions to Mars (see Asmar et al., 2009). The future radio links can be performed between an Orbiter and the Earth, the Earth and a Lander, and an Orbiter and a Lander. When we use the word "lander", the reader may as well replace it by "rover" if the rover is equipped with a precise motion-control system for its relative position (as foreseen on the ExoMars rover for instance).

Radio signals are often provided in multiple frequencies because they are perturbed when propagating through interplanetary media, particularly when the media are ionized. Since the perturbations induced by the solar corona or interplanetary plasma and the ionosphere of Mars and of the Earth depend on frequency, they can be corrected for by combining signals of

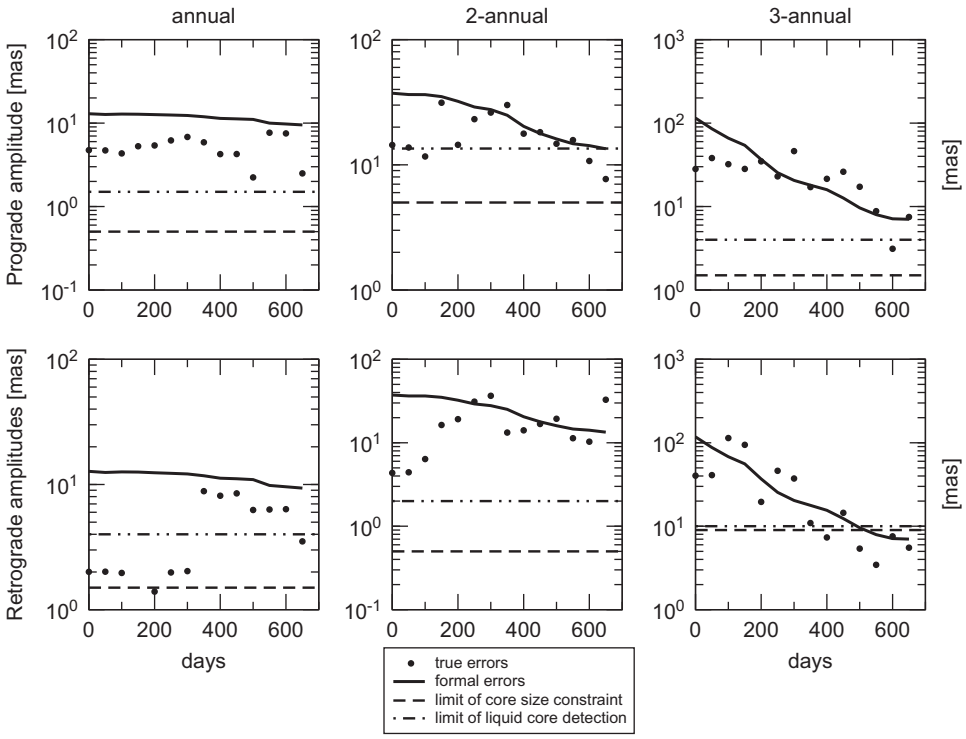

Fig. 4. Formal errors (full lines) and true errors (diamonds) on the amplitudes of the prograde and retrograde nutations determined from an X-band radio link between an equatorial lander and the Earth, as a function of the mission duration; the tracking is performed when the Earth is between 20° and 40° in the lander sky and for 45 min twice a week. The horizontal dotted lines indicate the amplitude above which one gets information concerning the core physical state and dimension from the nutation; the FCN and core radius considered for the simulated data are, respectively, 240 days and 1650 km.

Table 2
Frequencies allocated for the Space navigation/radioscience frequency band for Earth–space radio links at Mars.

Frequency band	Uplink (Earth to Space)	Downlink (Space to Earth)
S	[2.110 GHz, 2.120 GHz]	[2.290 GHz, 2.300 GHz]
X	[7.145 GHz, 7.190 GHz]	[8.400 GHz, 8.450 GHz]
Ka	[34.200 GHz, 34.700 GHz]	[31.800 GHz, 32.300 GHz]

Table 3
Frequencies allocated for the Space navigation/radioscience frequency band around Mars.

	Return frequency[a] Spacecraft to spacecraft	Forward frequency[a] Spacecraft to spacecraft
UHF	[390 MHz, 405 MHz]	[435 MHz, 450 MHz]

[a] 'Forward' usually means from the orbiter to the lander/rover and 'Return', from the lander/rover to the orbiter. But it is actually allowed to be reversed, and also allowed for an orbiter-to-orbiter link, so 'Forward' really means 'from the instrument that initiates the radio link' and 'Return' means 'instrument that locks onto a frequency from the originating radiolink instrument'.

different frequencies. Therefore, using different frequencies in one radio link helps in reaching the scientific objectives.

The radioscience data consist of Doppler and ranging measurements between a lander on Mars and a tracking station on Earth (consisting of antenna, receiver, emitter, reference clock, etc.), or between an orbiter around Mars and the Earth tracking station, or between an orbiter around Mars and a lander on Mars. The tracking stations on Earth operate primarily on two bands, S- and X-band. They were recently beginning to support a higher frequency, Ka-band, for some missions. We expect that Ka-band will be more and more used with X-band and that the S-band will be abandoned (Asmar et al., 2009). At present, the Orbiter–Lander links only use UHF. This has been the case for most landers and rovers that have been deposited at the surface of Mars, but we foresee that, in future missions, this link might also use the transponder on the lander provided for the Lander–Earth radio link at another frequency band such as X- or Ka-band (see Asmar et al., 2009).

The *Lander–Earth* links were regularly used for telemetry and telecommand in the past and present missions. Pathfinder (1997) for instance, used radio communication signals in X-band, compared with the S-band radio system used by the Viking landers. The Doppler data noise caused by solar plasma being inversely proportional to the square of the radio frequency, the Pathfinder Doppler data have about one order of magnitude less noise than the Viking lander Doppler data. This radiolink has then been used to determine the rotation of Mars (Folkner et al., 1997). In particular the radioscience data have been used to estimate improved values of the precession of Mars' pole of rotation and the variation in Mars' rotation rate. The MER rovers (Mars Exploration Rovers) use the UHF classical link with the orbiters for TMTC (telemetry/telecommunication) and regularly use as well the X-band Earth-lander link for commanding (in order to be independent on relay orbiters). This latter link was thus mainly used for TMTC but will be used for radioscience studies in the future when the MERs will be fixed at the surface of Mars. Communication from the short Phoenix mission has been performed through both X-band directly to Earth during cruise and through UHF relay via the US or ESA orbiters. Phoenix used UHF exclusively UHF during the landed mission for reasons related to energy requirement (also, in this case there was not too much visibility problem for the Phoenix–Orbiter radio links as the orbiters have all polar orbits). Future missions to Mars envisage direct-to-Earth X- and Ka-links with orbiters or landers at the

surface of Mars. For ExoMars an X-band coherent transponder called LaRa (for Lander Radioscience) has been developed (Dehant et al., 2009).

The *Orbiter–Earth* radio link has mostly been in X- and S-band (case of MarsExpress, for instance) but is now being replaced by X- and Ka-band links. The Cassini spacecraft uses X and Ka frequencies combined for the uplink and downlink in order to be able to correct the plasma effects on both uplink and downlink. Cassini radioscience is performed by two transponders: one transponder combining an X-band uplink and an X- and a Ka-band downlink, and another transponder in Ka-band (Ka-band uplink, Ka-band downlink). As far as missions to Mars are concerned, all recent US orbiters were equipped with X-band links and only MRO (Mars Reconnaissance Orbiter) has a Ka-band, which unfortunately failed working properly when the spacecraft was in orbit around Mars. It must be noted that Earth-to-space Ka-band capability is only supported by one NASA station at Goldstone presently. For future *network science* on Mars (mission called MarsNEXT or MarsNET at the ESA (European Space Agency) level), a very complete ensemble of radio links is proposed as presented in the next section. There are as well lander/rover to Orbiter X-band links envisaged in that mission.

A possible link scenario as foreseen in the MarsNet mission proposed to ESA is presented in Fig. 5. *For the Earth–Orbiter link* the ideal case would be to have X-band uplink/X-band downlink/Ka-band downlink as well as Ka-band uplink and downlink, as is the case for the Cassini spacecraft for the Earth–Orbiter link and will be for the BepiColombo mission. Both Ka-band and X-band are already supported by the DSN (Deep Space Network) stations of NASA and the ESTRACK (ESA Tracking stations) stations of ESA. With this configuration, the alteration experienced by the radio signal resulting from the plasma can be accounted for. As Mars has an ionosphere and as plasma may perturb the signal in the line-of-sight, similarly, it would be very useful to have the same configuration on the *Lander–Earth and Lander–Orbiter links*. However, current X/Ka-band transponders are too heavy to be incorporated on a small lander or rover. Instead, we envisage a miniaturized transponder in X-band (see Dehant et al., 2009) for these radio links as shown in Fig. 5. The X-band transponder has been proven to be feasible and very light. In order to be able to correct for the ionosphere and plasma effects, an additional Ka-band link is proposed (see Fig. 6). For a design using X-band for the uplink and X- and Ka-bands for the downlink, it is possible to correct for the plasma on the downlink and, when using this downlink plasma for the uplink plasma at another time in conjunction with plasma and ionosphere models, it is possible to decrease the plasma and ionosphere effects on the signal. Nevertheless, this method is still not perfect. It is preferable but more challenging to use a transponder totally in Ka-band (the technology at Ka-band is more delicate than at X-band). The design of such miniaturized Ka-band transponder is feasible but still under investigation. As proposed for the MarsNEXT (MarsNet), the use of such a lander transponder in X-band (or Ka-band or both), not only for the *Lander–Earth* link, but as well for the *Lander–Orbiter link* would improve significantly the scientific returns. An important improvement of multiple links or cross-links (see Figs. 5 and 6) over a single radio link from the lander is that the better coverage of the geometry of the different links can be used to improve the precision of all links (e.g. a factor two on the X-band noise level). As the uplink from Earth at around 7.15 GHz (X-band case) is different from the downlink at around of 8.45 GHz, it is not possible to use the existing hardware on the orbiter for this link. Indeed, the transponder on the surface of Mars receives at about 7.15 GHz and transmits back to Earth with the so-called transponder ratio at about 8.45 GHz; the instrument on board the orbiter receives at about 7.15 GHz and transmits back to Earth with the transponder ratio (which might be slightly different with respect to the Earth-Lander link) at about 8.45 GHz. Both cannot transmit at 7.15 GHz and cannot receive at 8.45 GHz. A dedicated design must be considered for this link.

The error sources on the Lander–Earth link are shown as an example in Table 4 for X-band. They are related to the thermal noise as well as the media in the line-of-sight, in particular the solar plasma effects and the Earth troposphere and ionosphere

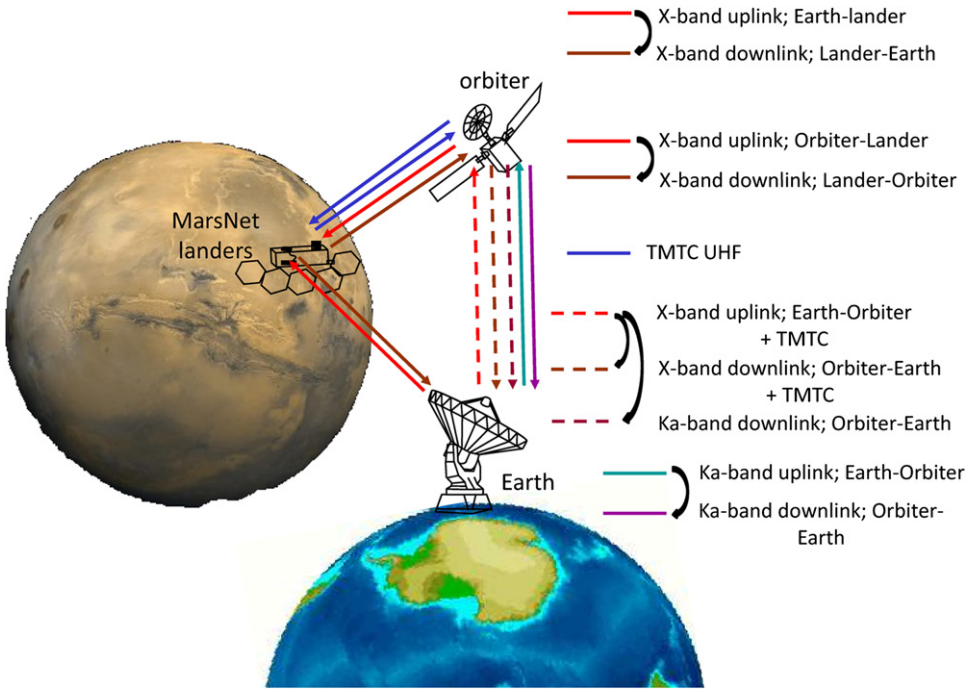

Fig. 5. Possible frequency bands for the radio links between Mars and the Earth. The dashed lines in the Earth–orbiter link correspond to the nominal radiolink starting from an X-band uplink, multiplied to an X-band downlink and a Ka-band downlink. The full lines in the Earth–Orbiter link correspond to an optional Ka-band uplink and a Ka-band downlink.

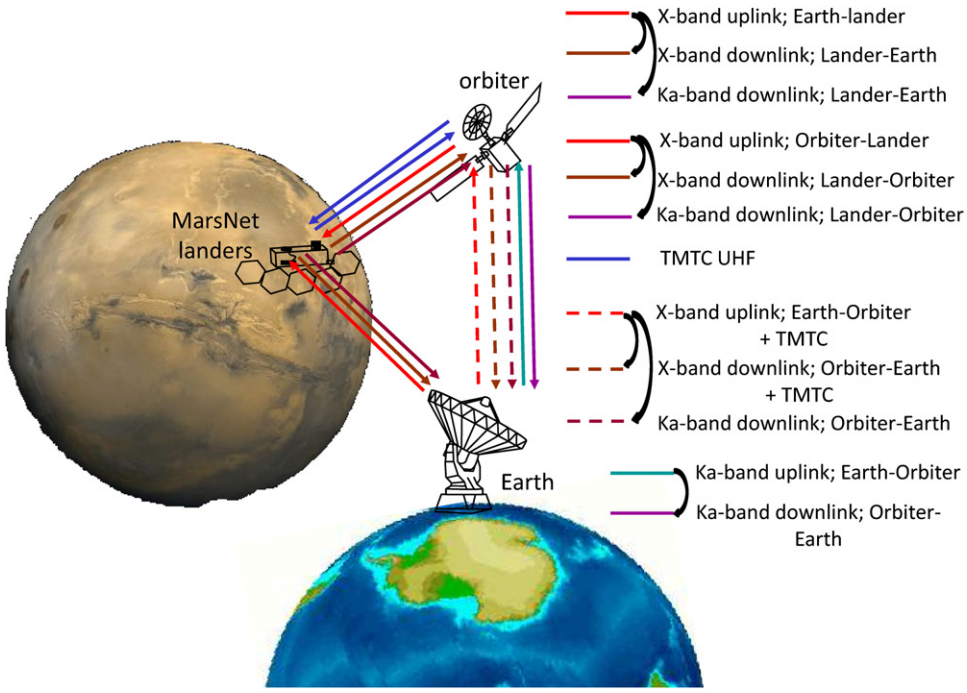

Fig. 6. Possible frequency bands for the radio links between Mars and the Earth, including Ka-band radio links. There are additional links in Ka-band with the lander, with respect to Fig. 5.

Table 4
Error sources for a transponder used for the Lander–Earth radio link. If scintillations in the solar plasma are taken into account, the plasma noise can reach 0.04 mm/s and the total noise can reach more than 0.05 mm/s.

Error sources	Level on the Doppler at 60 s integration time; in mm/s
Thermal noise of the transponder (from LaRa link budget and industry requirements)	0.02
Nominal Solar plasma effects at 5° elongation (Nkono et al., in preparation)	0.015
Ionosphere effects (including scintillations)	0.02
Remaining troposphere at 30° elevation angle after dry troposphere corrections from model explaining 90% of the effect: from 0.060 to 0.006	0.01
Total root mean square	0.034

perturbations. The estimation of the *thermal noise contribution* (due to the finite value of SNR on the radio links) is based on the following assumptions: (1) a measurement integration time of 60 s; the typical values used for the Doppler data is in the range [60–180 s] of which the lower bound corresponds to the worst case; (2) a bandwidth of the deep space station carrier loop bandwidth of 3 Hz that we have chosen small compared with the transponder carrier loop bandwidth (30 Hz) and in agreement with latest transponder design (such as the LaRa transponder for ExoMars); (3) considering the distance Earth–Mars we have taken the worst case (large distance Earth–Mars) to determine the power to noise spectral density ratio (uplink and downlink) required to estimate the measurement error caused by the phase jitter introduced by both the transponder and the deep space station receivers. Concerning the microwave carrier phase scintillations induced by the *solar corona*, we have supposed as an example for Table 4 that for a Sun–Earth-probe angle of 5°. The solar plasma or solar wind stream of charged particles ejected from the Sun is divided into two components, respectively termed the slow solar wind (velocity of about 400 km/s) and the fast solar wind (velocity of 750 km/s). The slow solar wind is twice denser and more variable in intensity than the fast solar wind. The slow wind also has a more complex structure, with turbulent regions and large-scale structures. Both the fast and slow solar winds can be interrupted by large, fast-moving bursts of plasma (solar storms) called interplanetary coronal mass ejections or CMEs. These different wind streams form a spiral. We have supposed that the major undesired effects on the time delay due to the presence of an ionized medium could be removed thanks to current models that provide good indications of the solar wind electron density distribution and that the remaining errors are at the level of 0.015 mm/s at 5° elongation for usual X-band link with a 10 s integration time (Nkono et al., in preparation). Concerning the *ionosphere*, we have also supposed that the major undesired effects on the time delay/Doppler phase could be removed thanks to current models and that the remaining error sources come from unpredictable scintillations of which the contribution has been evaluated for an elevation of 30° (TEC standard deviation $\sim 4\times10^{15}$ e-/m^2) with $T=60$ s. Finally, we have also assumed that the standard tropospheric models could explain 90% (the dry part of the atmospheric contribution) of the effects observed during the propagation of the signal in the neutral atmosphere layer and that the remaining unmodeled contribution is related to the water vapor content in the atmosphere.

The solar plasma is presently the major remaining error source for radioscience (see Nkono et al., in preparation). Table 4 shows the contributions for a particular elongation angle of 5° (the elongation angle is the angle between the planet and the Sun, as viewed from the Earth.) For another elongation angle closer to the Sun, the plasma effects will be larger (see Nkono et al., in preparation). If models are considered, it is possible to correct for the interplanetary plasma effects at X- or Ka-bands for elongation angles larger than a few degrees. However, without the use of two frequency combination, it is impossible to correct for the solar corona or plasma effects at elongation angles close to the Sun. Plasma scintillations, in addition to the plasma classical

repartition described above, may exist especially when there is high solar activity. Solar corona mass ejection (CME) may significantly perturb the radio signal. Because of the large improvement in signal to noise ratio for the Ka band and the smaller sensitivity of the radio link on the plasma effects we can expect to get a number of loss of lock lower in Ka-band than in X-band. An uplink in X-band combined with two downlinks in X- and Ka-bands would be convenient as well though will not help in the loss of lock if only X-band uplink is used (X-band is more sensitive than Ka-band for the effect of scintillations); while the downlink plasma effects will be corrected from the combination of X- and Ka-bands, only an estimation of the uplink solar plasma contribution will be possible. Fig. 6 shows this possibility related to the addition of a Ka-band downlink for the Lander–Earth link (or equivalently Rover–Earth link). The figure shows as well an additional Ka-band for the Lander–Orbiter link, but for geodesy, there is probably no significant charge particle effect at X-band from the Martian ionosphere and so no advantage to have Ka-band for that link. Additionally the consideration of a downlink from the Orbiter to the Lander at the same frequency band as the receiving frequency from Earth, i.e. the uplink frequency from Earth to the Orbiter may lead to instrumental problems and may not be allowed as the receiving channel from Earth must be free for any uploaded command to the spacecraft.

As proposed in Table 4, the precision of future radioscience experiments will be at the level of 0.035 mm/s at 60 s integration time in X-band. The solar plasma effect is strongly dependent on solar elongation; in practice one consider to putting in some limits on the elongation angle when considering observations schedule. At elongation angles greater than about 20°, which is true most of the time, the effect of solar plasma on Ka-band signals is lower than other noise sources so multiple frequencies need not be used if consistent with the science experiment. This limit of elongation angle for the X-band only might be a little bit higher. The solar plasma effects considered for that table is very small (nominal situation for large elongation angles). We have considered that the noise contribution can be tripled and corresponds to a 0.05 mm/s precision on the Doppler measurements used in our simulations in X-band, providing a limit of the elongation angle at 20°. With this precision, it is thought possible to obtain the nutation amplitudes and therewith the physical state and dimension of the core (Dehant et al., 2009) and, if a lander–orbiter radiolink is implemented and/or if high precision orbits can be determined for the orbiter, it will be possible to obtain a better value of the k_2 Love number. Therewith, a confirmation that the core is liquid (or partially liquid) will be possible and the uncertainties on the core size and on the concentration of light elements in the core will be reduced significantly.

The precision of the future radioscience observation using lander(s) or rover(s) (when these have a motion-control system) could in principle allow in addition to measure the deformation of the surface of Mars (tidal deformation of atmospheric loading) when observing at a high precision. Our simulations have shown that the few centimeter level may be reached in the time domain with X-band (even a factor at least two better with Ka-band transponder on a lander) and our computations have shown that tidal displacement may reach a couple of centimeters peak-to-peak depending on the landing site. Tides are forced by the gravitational forcing of the Sun mainly (Phobos and Deimos and the other planets of the solar system induce also tides but the total contributions are below the centimeter level). This gravitational forcing is almost perfectly known, better than the sub-millimeter level (Roosbeek, 2000). A rough estimation of their order of magnitude with a comparison with the Earth tides, leads to the following deductions: (1) the tidal potential being inversely proportional to the distance and proportional to the radius of the planet, its value for Mars is about 7% of that of the Earth and the ratio between the tidal potential and the gravity providing the surface displacement roughly reaches the level of a few centimeters. This has been fully developed by Van Hoolst et al. (2003). The tidal displacements do not only depend on the gravitational forcing but also on the interior of Mars. The presence of a liquid or partially liquid core and the dimension of the core largely influence the response of Mars to the gravitational forcing. This response is characterized by the tidal Love number h_2. It represents the periodic tidal radial displacement of the planet and can be obtained in principle from the displacement along the line of sight (for favorable geometry when the radial contribution to the line-of-sight is not zero). We must as well consider the landing site position in the three dimensions for a full picture of all tidal contributions (see Van Hoolst et al., 2003). The tidal contributions to the displacement of the surface are larger for a liquid core than for a solid core and increases when the core radius increases. For example, for the radial contribution represented by h_2, increasing the core radius by 300 km (which is within the present uncertainties) increases h_2 by about 34%, and changing to a solid core decreases it by 30%, which provides variations that may correspond to doubling the values of the tidal displacement when considering a solid core and a large liquid core. This shows the full potential of observing the tides. The absence of a global magnetic field suggests that the core of Mars is entirely liquid (see e.g. Breuer and Spohn, 2003, 2006). If Mars were nevertheless to have a solid inner core, its presence would be difficult to observe, in particular when the inner core is small. The presence of an inner core could then be inferred indirectly from the percentage of light element within the core, the thermodynamical properties of the core constituents, and from the temperature and pressure conditions inside the core.

Additionally, the atmosphere above a lander changes and therefore induces additional changes in the displacements of the lander due to the atmospheric mass loading (Van Hoolst et al., 2002; Karatekin et al., 2006a; Métivier et al., 2008). The seasonal changes in the atmosphere and ice caps related to the CO_2 sublimation and condensation process is a global phenomenon that affects the pressure enormously; one fourth of the atmosphere is participating into this seasonal phenomena. Because of this seasonal mass exchange between the north and south polar caps, the largest surface displacement is associated with changes of the mass center of the 'solid' planet (without atmosphere) in the north–south direction and amounts to 6.5 centimeters peak-to-peak (Van Hoolst et al., 2002). Other loading contributions to the surface displacement are below 1 cm (Métivier et al., 2008). Since the degree-one (center of mass) displacement is not very sensitive to the internal properties of Mars, one can conclude that loading effects on a lander displacement must be accounted for in the computation but will most probably not help the determination of the core properties. Only the lander tidal displacements measured with high precision radioscience transponders (e.g. a few tens of micrometers per second on the Doppler shift on X-band) can be used in conjunction with other measurements in order to obtain important information on the core state, composition, and dimension and therewith on Mars' evolution. As for the tidal contributions, the inner core influence on the loading Love number is very small and not observable as Mars response to loading is mostly driven by the mantle rheological properties.

In addition, the radioscience observation will allow us to determine the length-of-day variations (ΔLOD) and polar motion and therewith to constrain the mass involved in the CO_2 sublimation/condensation process. It is expected that the results from cross-signals involving both a lander (or rover) and an orbiter tracked from Earth as well as a Lander–Orbiter (or Rover–Orbiter) link, have a

higher precision than those resulting from a direct link from the surface of Mars to the Earth only when the orbiter has a Ka-band tracking system (when the precise orbits are at the meter or 10-cm level). The covered geometry with a Lander–Orbiter link is better than the geometry of a direct-to-Earth link. However the imprecision of the orbit of the orbiter in the case of a Lander–Orbiter link will directly map into the precision of the Lander positioning. The present paper concentrates on the results on the interior of Mars, the CO_2 cycle being treated in another paper of this special issue (see Karatekin et al., this issue). However, it is worth mentioning that polar motion and length-of-day variations are also influenced by the deformation of the planet induced by the changes in the atmospheric masses. For example, differences between the length-of-day variations for a solid core and for a liquid core are at the percent level (Karatekin et al., 2005b). Measurements of ΔLOD must have an accuracy better than 2% to determine whether or not the core is liquid, and even better ($<0.5\%$) to constrain the core size. The precision on the length-of-day measurements depends on the relative positions of a lander, the Earth, and possibly the orbiter and depends as well on the line-of-sight of the observation (mainly the elevation of the Earth or the orbiter in the sky of the lander). In addition to the sensitivity of the Doppler measurements to the geophysical parameters, the noise level on the observations must be very low and in particular the plasma noise contribution that was discussed in Section 1. This will only be possible with very high precision transponders (signal-to-noise ratio at a few dB level and Doppler velocity at a few micrometer level) that will have either very high frequency such as Ka-band or combination of frequencies.

Table 5 below summarizes the main characteristics and objectives of a transponder at the surface of Mars for a 180 days minimum period in order to reach the geodetic objectives explained above. The last row was provided for completeness but is not discussed in this paper but rather in Karatekin et al. (this issue).

5. Orbiter–Earth radio link and information on the interior from rotation and tides

An improvement of the radiolink between an orbiter and the Earth could in principle allow for a better determination of the k_2 value. In particular, the addition of a Ka-band in the radio links between the Earth and the orbiter would increase the precision of the measurements (and thus on the orbit parameter determination) by one order of magnitude (i.e. at the 10 cm level for precise orbit determination) and, with it, will improve the precision on the determination of the Love number k_2 by about the same order of magnitude. It must be noted however that the precision depends also on the tracking of the spacecraft that is ideally almost continuous in order to be able to correct for all the non-gravitational effects on the spacecraft, in particular when wheel-off-loading desaturation or angular momentum desaturation maneuvers are performed. The length of the measurement series is also important. If one considers that the total range of uncertainty on k_2 is presently the extreme values of the ranges obtained by the different radioscience teams, then the k_2 value is determined with a relative precision of about 30–50%. A gain of one order of magnitude on this value would lead to a precision on the estimated core radius of a few tens of km as can be deduced from Fig. 11 of Dehant et al. (2009) and as discussed in Rivoldini et al. (2010). This precision would allow obtaining information about the existence of a phase transition at the bottom of the mantle. For instance, if the core size is such that the pressure condition and temperature conditions would not allow the phase transition (large core), this question may be definitely answered. However, it must be mentioned that, for some core sizes (smaller core), it will not be possible to decide due to the combined uncertainties on the mantle temperature and mineralogy and on the Clapeyron slope of the perovskite transition (Van Thienen et al., 2006, 2007; Mocquet et al., 2010).

The addition of a Lander–Orbiter link to the Orbiter–Earth link will further allow improving the determination of the Love number k_2.This will be jointly used with the information derived from nutation in order to better constrain the models of the interior of Mars.

Additionally, there are secular/long-period contributions of k_2 on high-precision orbit parameters (from the zonal tides or from secular part of the tidal effects) as well as the periodic contributions (from tesseral and sectorial tidal effects), which can be seen on high-precision tracking data. The secular/long-period contributions of k_2 to the precise orbit determination will be improved if the time-variable gravity (CO_2 cycle) is better determined. Indeed, the secular/long-period contributions of the tidal Love number k_2 and the time-variable degree-two gravity coefficient ΔJ_2 are highly correlated and in parallel ΔJ_2 is highly

Table 5
Main characteristics of radioscience measurements from Lander–Earth radio link.

Science objectives	Scientific measurement requirements	Instrument functional requirements	Mission functional requirements
Characterize the Martian core size, density, and state.	Determination of the polar moment of inertia and precession rate to accuracy better than 0.1%. Measurement of nutation amplitudes with accuracy of a few milliarcseconds or better. Determination of the tidal displacements at centimeter level or better. Determination of the annual and semi-annual variations in planetary moment of inertia by measuring seasonal length-of-day variations with accuracy better than 0.01 ms.	Determination of distance of lander to spin axis of date with an accuracy of 2 cm or better and lander longitude of date with an accuracy of 2 milliarcseconds or better from one day of Doppler tracking. X-band and Ka-band carrier signal from Earth with stability better than 10^{-13} over time scales of 10–1000 s with equivalent isotropic radiated power greater than 6 W.	Power on X-band and Ka-band lander radioscience transponder for e.g. 45 min-long tracks twice per week for two Earth years (180 days minimum). Use DSN antennas to transmit and receive signal and measure Doppler shift to accuracy better than 10^{-13} corresponding to about 0.05 mm/s at 60 sec integration time.
Characterize the Martian mantle density and structure (infer composition).	Determination of the polar moment of inertia and precession rate to accuracy better than 0.1%. Measurement of nutation amplitudes with accuracy of a few milliarcseconds.		
Characterize seasonal CO_2 mass exchange between atmosphere and polar caps.	Determine annual and semi-annual variations in planetary moment of inertia by measuring seasonal length-of-day variations with accuracy better than 0.1 ms.		

correlated to ΔLOD (see Duron et al., 2003). Furthermore, Lander–Earth measurements will improve the present ΔLOD determination at least by one order of magnitude for a mission duration of one year. This can be even better for a Lander–orbiter link and will provide important constraints on CO_2 cycle, provided that the relatively small atmospheric contribution to ΔLOD induced by the atmospheric wind is deduced from other kinds of observations and/or GCM simulations (Montabone et al., 2006; Forget et al., 1999; Spiga and Forget, 2009). The k_2 value can thus be better determined independently from the time variations of the degree-two gravity coefficient J_2 (ΔJ_2) and the length-of-day variations (ΔLOD). These considerations are based on low polar orbit spacecraft (~500 km altitude); other inclinations for the orbit could be even better (Karatekin et al., 2005a). These qualitative studies must still be completed by numerical simulations, which will be shown elsewhere (see Rosenblatt and Dehant, 2010). The k_2 value associated with the mass repartition inside the planet related to the tides can then be determined by using the observed k_2 value and correcting it for the atmospheric loading contribution.

It is also interesting to consider, in addition to the Lander–Earth radio link, a Lander–Orbiter link to improve the determination of nutations and length-of-day variations. Here again the geometry of the orbit and the position of the lander are of prime importance. In particular for an equatorial orbit observing an equatorial lander, the nutations will be best determined (the contribution to the Doppler shift is maximized when the orbiter inclination and the lander latitude are small), while for a polar lander observed from a polar orbit, the polar motion is better determined (Yseboodt et al., 2003).

In the frame of this paper we present two simulations performed with a semi-analytical method, with an equatorial lander at 10° longitude, with Doppler measurements twice per week, and a noise at the level of 0.05 mm/s; the first simulation considers a direct link to the Earth and the second one, a Lander–orbiter link with a spacecraft orbit at an altitude of 500 km with an eccentricity of 0.02 (pericenter at 422 km, apocenter at 578 km) and an inclination of 85°. The figures (Figs. 7 and 8) presented in the frame of these simulations show, for each parameter, the 'true error', which is the difference between its estimated value with respect to its 'truth' value (value that we use to simulate the data). The parameters considered in these simulations are similar to those used in Yseboodt et al. (2003):

(1) the core factor F, i.e. the amplitude of the resonance to the Free core nutation (FCN) in the nutation response (the nutation amplitude for the non-rigid Mars takes the form of a rigid-Mars nutation amplitude times the $(1+F\,\sigma/(\sigma-\sigma_0))$ factor, where σ is the prograde or retrograde nutation frequency);
(2) σ_0, the FCN frequency;
(3) the amplitude of the cosine and sine of the semi-annual and annual seasonal changes in Mars rotation;
(4) the precession rate;
(5) the lander latitude and longitude; and
(6) the lander altitude.

Fig. 7 shows the results for the Lander–Earth link as a function of the mission duration up to one Martian year and Fig. 8 for the Lander–Orbiter link. In these simulations we have evaluated the resonance amplification factor and the resonance FCN frequency, the precession rate, the amplitude of the seasonal LOD changes, and the lander position. The comparison of the two figures allows to conclude that with radio links at the same level of performance and even with a degradation of the precise orbit of the orbiter, the Lander–orbiter link provides better performances; this is due to the geometry covered by the line-of-sight of the Doppler shift measured. For instance, one observes that the resonance amplification factor related to the core moment of inertia and the FCN period are determined more rapidly (after about 150 days) in the lander–orbiter–Earth case than in the lander–Earth case (after 400 days), and similarly for the lander position.

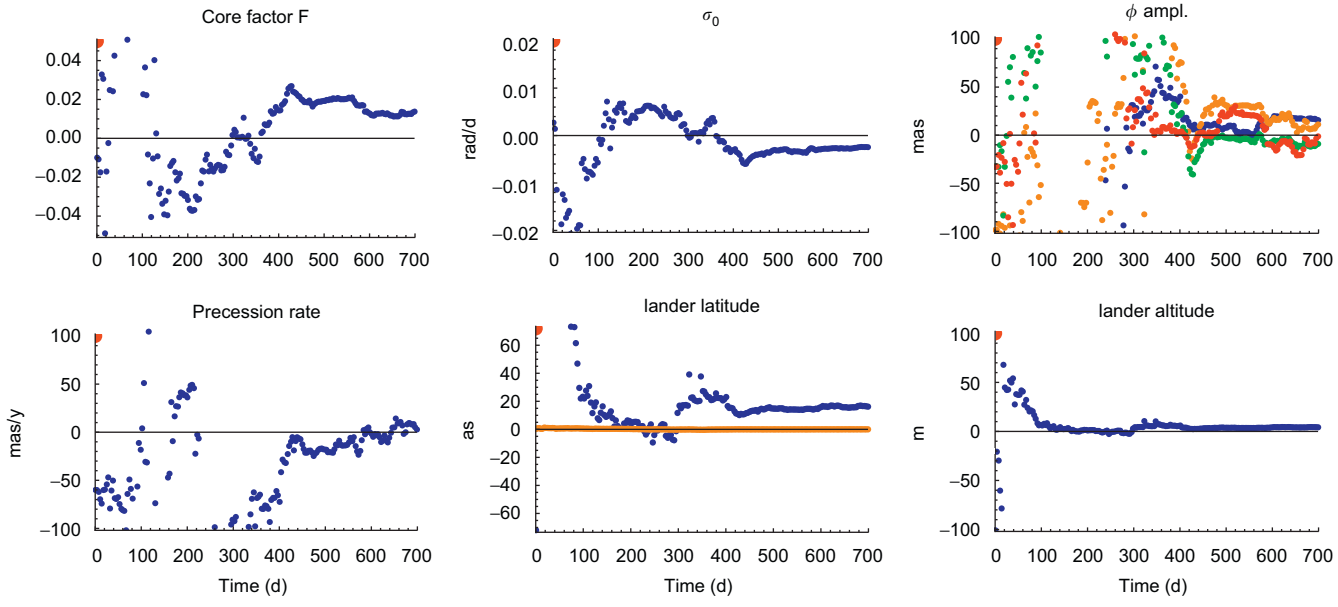

Fig. 7. Parameter estimation (FCN amplification factor (F), FCN frequency (σ_0), four amplitudes of cosines and sines in UT seasonal changes (ϕ ampl.), precession rate, and lander coordinates (latitude, longitude, and altitude) as a function of the mission lifetime) for a simulation using a noise level of 0.05 mm/s on the Doppler for a direct lander–Earth link. In the graph providing the seasonal changes in the rotation ϕ ampl., the four curves correspond to cosine and sine of the annual changes (blue and orange), respectively, and to cosine and sine of the semi-annual change (green and red). In the graph providing the lander latitude, blue means latitude an orange means longitude. (For interpretation of the references to colour in this figure legend, the reader is referred to the web version of this article.)

6. Conclusions

With radioscience involving lander–Earth or orbiter–Earth or orbiter–lander links, one has access to tides, precession, nutation, polar motion, length-of-day, and therewith to properties of Mars' interior.

From precession and nutation, it will be possible to obtain the moments of inertia of the whole planet, of its core and its mantle, as well as Mars' core state and dimension, important constraints on Mars' evolution.

From tidal effects on the orbiter preferably with a non-polar orbit, it will be possible to better constrain the tidal Love number k_2. The atmospheric contribution to the measurements must be corrected for before any interpretation in terms of physics of Mars' interior. A better determination of the low-degree gravity coefficients and of the length-of-day variations will further help this determination. The sublimation and condensation of CO_2 in the atmosphere and ice caps affect indeed the gravity and the length-of-day, as well as by a loading effect on the planet's mass repartition inside the planet.

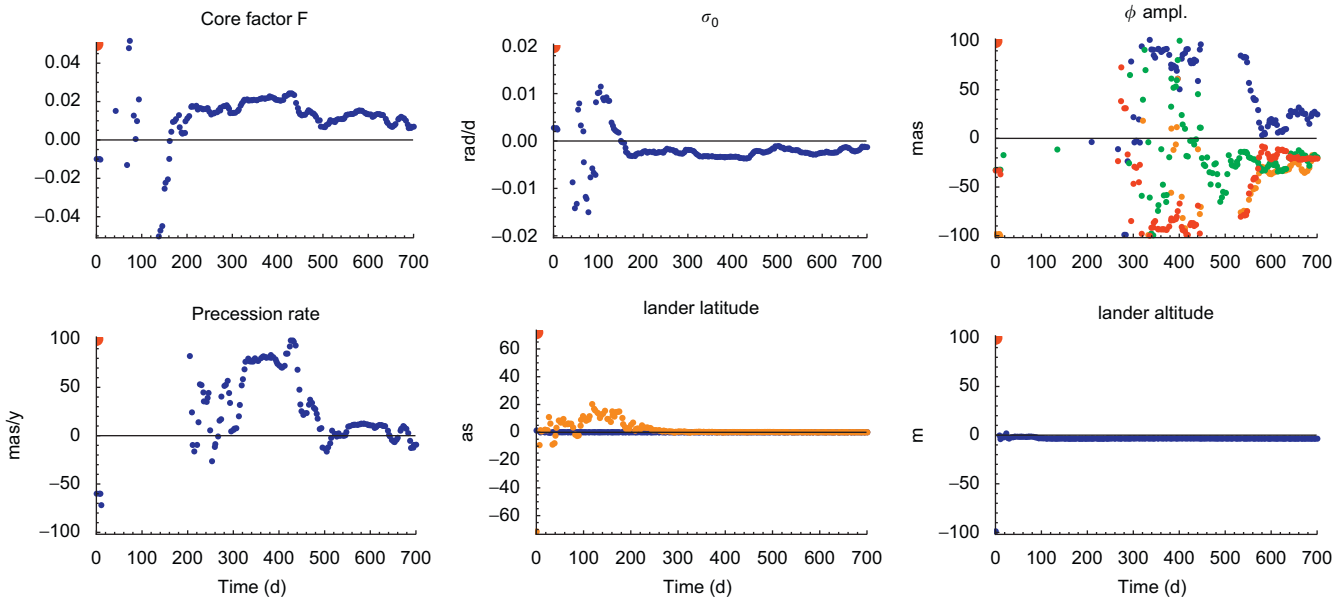

Fig. 8. Parameter estimation (FCN amplification factor (F), FCN frequency (σ_0), four amplitudes of cosines and sines in UT seasonal changes (ϕ ampl.), precession rate, and lander coordinates (latitude, longitude, and altitude) as a function of the mission lifetime) for a simulation using a noise level of 0.05 mm/s on the Doppler for a lander–Orbiter link. In the graph providing the seasonal changes in the rotation ϕ ampl., the four curves correspond to cosine and sine of the annual changes (blue and orange), respectively, and to cosine and sine of the semi-annual change (green and red). In the graph providing the lander latitude, blue means latitude an orange means longitude. (For interpretation of the references to colour in this figure legend, the reader is referred to the web version of this article.)

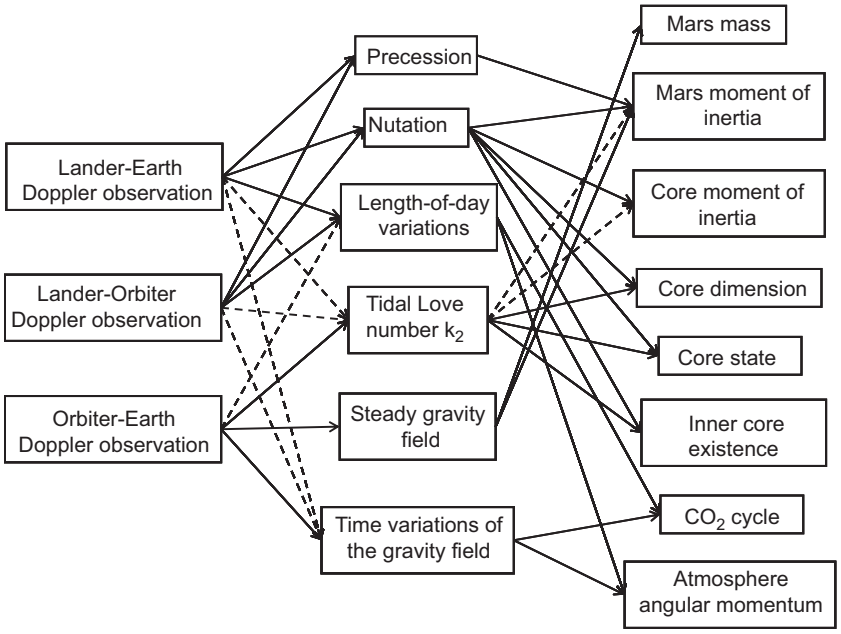

Fig. 9. Summary of the observation and the results that will be obtained with radioscience.

Fig. 9 summarizes all the results that can be obtained from radioscience. It shows the high interdependence of all the phenomena. It shows that, when we will be able to perform high-level radioscience measurements, only a careful processing of the data will allow a step forward in our understanding of Mars' deep interior. Future mission opportunities such as ExoMars (rover on Mars) and MarsNEXT (network of landers on Mars and high-performance radio links on the orbiter) may well lead to reach these objectives.

However, the precision that will be reached in the future with the combination of different links is very much depending on the geometry of the whole sets of instruments, i.e. the position of the lander/rover at the surface of Mars or the orbital elements of the orbiter.

Acknowledgements

This work was financially supported by the Belgian PRODEX program managed by the European Space Agency in collaboration with the Belgian Federal Science Policy Office. J.C. Marty was supported by the CNES Program Directorate. We also thank very much Bill Folkner, Bert Vermeersen, and Frank Sohl for their constructive review of our manuscript.

References

Asmar, S., and more than 10 authors, 2009. Planetary Radio Science: Investigations of Interiors, Surfaces, Atmospheres, Rings, and Environments. White Paper submitted to the 2009 Planetary Sciences Decadal Survey, 8 p.

Balmino, G., Duron, J., Marty, J.C., Karatekin, Ö., 2006. Mars long wavelength gravity field time variations; a new solution from MGS tracking data. In: Proceedings of the IAG Symposium 2005 on 'Dynamic planet', Cairns, Australia, vol. 125, pp. 895–902.

Barriot, J.P., Dehant, V., Cerisier, J.-C., Folkner, W., Rhibes, A., Benoist, J., Van Hoolst, T., Warnant, R., Preston, R.A., Romans, L., Wu, S., Wernik, A.W., 2001. NEIGE: NetLander ionosphere and geodesy experiment. Adv. Space Res. 28 (8), 1237–1249.

Bertka, C.M., Fei, Y., 1998. Density profile of an SNC model Martian interior and the moment-of-inertia factor of Mars. Earth Planet. Sci. Lett. 157 (1–2), 79–88, doi:10.1016/S0012-821X(98)00030-2.

Breuer, D., Yuen, D.A., Spohn, T., 1997. Phase transitions in the Martian mantle: implications for partially layered convection. Earth Planet. Sci. Lett. 148 (3–4), 457–469, doi:10.1016/S0012-821X(97)00049-6.

Breuer, D., Spohn, T., 2003. Early plate tectonics versus single-plate tectonics on Mars: evidence from magnetic field history and crust evolution. J. Geophys. Res. 108, 8–11, doi:10.1029/2002JE001999.

Breuer, D., Spohn, T., 2006. Viscosity of the Martian mantle and its initial temperature: constraints from crust formation history and the evolution of the magnetic field. Planet. Space Sci. 54, 153–169, doi:10.1016/j.pss.2005.08.008.

Defraigne, P., de Viron, O., Dehant, V., Van Hoolst, T., Hourdin, F., 2000. Mars rotation variations induced by atmospheric CO_2 and winds. J. Geophys. Res. (Planets) 105 (E10), 24,563–24,570.

Defraigne, P., Rivolidini, A., Van Hoolst, T., Dehant, V., 2003. Mars nutation resonance due to free inner core nutation. J. Geophys. Res. 108 (E12), 5128, doi:10.1029/2003JE002145.

Dehant, V., Defraigne, P., Van Hoolst, T., 2000a. Computation of Mars' transfer function for nutation tides and surface loading. Phys. Earth Planet. Inter. 117, 385–395.

Dehant, V., Van Hoolst, T., Defraigne, P., 2000b. Comparison between the nutations of the planet Mars and the nutations of the Earth. Survey Geophys. 21 (1), 89–110.

Dehant, V., Van Hoolst, T., de Viron, O., Greff-Lefftz, M., Legros, H., Defraigne, P., 2003. Can a solid inner core of Mars be detected from observations of polar motion and nutation of Mars? J. Geophys. Res. (Planets) 108 (E12), doi:10.1029/2003JE002140.

Dehant, V., Lognonné, Ph, Sotin, C., 2004. Network science, NetLander: a European mission to study the planet Mars. Planet. Space Sci. 52 (11), 977–985.

Dehant, V., Folkner, W., Renotte, E., Orban, D., Asmar, S., Balmino, G., Barriot, J.P., Benoist, J., Biancale, R., Biele, J., Budnik, F., Burger, S., de Viron, O., Häusler, B., Karatekin, Ö., Le Maistre, S., Lognonné, P., Menvielle, M., Mitrovic, M., Pätzold, M., Rivoldini, A., Rosenblatt, P., Schubert, G., Spohn, T., Tortora, P., Van Hoolst, T., Witasse, O., Yseboodt, M., 2009. Lander radioscience for obtaining the rotation and orientation of Mars. Planet. Space Sci. 57, 1050–1067, doi:10.1016/j.pss.2008.08.009.

Dreibus, G., Wänke, H., 1985. Mars, a volatile-rich planet. Meteoritics 20 (2), 367–381, doi:10.1016/0019-1035(87)90148-5.

Dreibus, G., Wänke, H., 1987. Volatiles on Earth and Mars—a comparison. Icarus 71, 225–240.

Duron, J., Rosenblatt, P., Yseboodt, M., Karatekin, O., Dehant, V., Van Hoolst, T., Barriot, J.-P., 2003. Joint estimation of Martian C20 and rotation variations from simultaneous geodetic measurements: Numerical simulations of a Network Science Experiment. Geophys. Res. Lett. 30 (18), 1971, doi:10.1029/2003JL082003.

Folkner, W.M., Yoder, C.F., Yuan, D.N., Standish, E.M., Preston, R.A., 1997. Interior structure and seasonal mass redistribution of mars from radio tracking of Mars pathfinder. Science 278 (5344), 1749.

Forget, F., Hourdin, F., Fournier, R., Hourdin, C., Talagrand, O., Collins, M., Lewis, S.R., Read, P.L., Huot, J.-P., 1999. Improved general circulation models of the Martian atmosphere from the surface to above 80km. J. Geophys. Res. 104 (E10), 24,155-24,176.

Grott, M., Helbert, J., Nadalini, R., 2007. Thermal structure of Martian soil and the measurability of the planetary heat flow. J. Geophys. Res. 112, E09004, doi:10.1029/2007JE002905.

Harri, A.M., Marsal, O., Leppelmeier, G.W., Lognonne, P., Glassmeier, K.-H., Angrilli, F., Banerdt, W.B., Barriot, J.P., Bertaux, J.L., Berthelier, J.J, Calcutt, S., Cerisier, J.C., Crisp, D., Dehant, V., Di Pippo, S., Giardini, D., Guerrier, D., Jaumann, R., Kumpulainen, K., Langevin, Y., Larsen, S., Menvielle, M., Musmann, G., Polkko, J., Pommereau, J.P., Runavot, J., Schumacher, W., Siili, T., Simola, S., Tillman, J.E., 1999. Network science landers for Mars. Adv. Space Res. 23 (11), 1915–1924.

Karatekin, Ö., Duron, J., Rosenblatt, P., Van Hoolst, T., Dehant, V., Barriot, J.P., 2005a. Mars' time-variable gravity and its determination: simulated geodesy experiments. J. Geophys. Res. (Planets) 110 (E6), E06001, doi:10.1029/2004JE002378.

Karatekin, Ö., Van Hoolst, T., Tastet, J., de Viron, O., Dehant, V., 2005b. The effects of seasonal mass redistribution and interior structure on length-of-day variations of Mars. Adv. Space Res., doi:JASR-D-04-01301.

Karatekin, Ö., Hagedoorn, J., Van Hoolst, T., Dehant, V., 2006a. Displacement of Martian surface due to seasonal surface mass redistribution and its detection from lander–orbiter–Earth links, In: Proceedings of the Fourth Mars Polar Science Conference, extended abstract no: 8039.

Karatekin, Ö., Van Hoolst, T., Tastet, J., de Viron, O., Dehant, V., 2006b. The effects of seasonal mass redistribution and interior structure on length-of-day variations of Mars. Adv. Space Res. 38 (4), 739–744, doi:JASR-D-04-01301R1.

Karatekin, Ö., de Viron, O., Lambert, S., Dehant, V., Van Hoolst, T., Atmospheric angular momentum variations of Earth, Mars and Venus. Planet. Space Sci., this issue.

Konopliv, A.S., Yoder, C., Standish, E.M., Yuan, Dah-Ning, Sjogren, W.L., 2006. A global solution for the Mars static and seasonal gravity, Mars orientation, Phobos and Deimos masses, and Mars ephemeris. Icarus 182 (1), 23–50, doi:10.1016/j.icarus.2005.12.025.

Konopliv, A.S., Asmar, S.W., Folkner, W.M., Karatekin, Ö., Nunes, C., Smrekar, D.S.E., Yoder, C.F., Zuber, M.T., Mars high resolution gravity fields from MRO, Mars seasonal gravity, and other dynamical parameters. Icarus, in press.

Le Maistre, S., Rosenblatt, P., Dehant, V., Marty, J.C., Rivoldini, A., Lander radio science experiment with a direct link between Mars and the Earth. Icarus, submitted for publication.

Lognonné, P., Giardini, D., Banerdt, B., Gagnepain-Beyneix, J., Mocquet, A., Spohn, T., Karczewski, J.F., Schibler, P., Cacho, S., Pike, T., Cavoit, C., Desautez, A., Pinassaud, J., Breuer, D., Campillo, M., Defraigne, P., Dehant, V., Deschamp, A., Hinderer, J., Leveque, J.J., Montagner, J.P., Oberst, J., 1999. The NetLander very broad band seismometer. Planet. Space Sci. 48 (12–14), 1289–1302.

Marty, J.C., Duron, J., Balmino, G., Dehant, V., Rosenblatt, P., Van Hoolst, T., 2009. Martian gravity field model and its time variations. Planet. Space Sci. 57 (3), 350–363, doi:10.1016/j.pss.2009.01.004.

Métivier, L., Karatekin, Ö., Dehant, V., 2008. The effect of the internal structure of Mars on its seasonal loading deformations. Icarus 194 (2), 476–486, doi:10.1016/j.icarus.2007.12.001.

Mocquet, A., Rosenblatt, P., Dehant, V., Verhoeven, O., 2010. The deep interior of Venus, Mars, and the Earth: a brief review and the need for surface-based measurements. Planet. Space Sci., this issue, doi:10.1016/j.pss.2010.02.002.

Montabone, L., Lewis, S.R., Read, P.L., Hinson, D.P., 2006. Validation of martian meteorological data assimilation for MGS/TES using radio occultation measurements. Icarus 185 (1), 113–132, doi:10.1016/j.icarus.2006.07.012.

Nkono, C., Rosenblatt, P., Dehant, V., Zhukov, A., Mitrovic, M., Bird, M., Le Maistre, S., Quantification of Solar corona effects on radio frequency waves, in preparation.

Pätzold, M., Tellmann, S., Andert, T., Carone, L., Fels, M., Schaa, R., Stanzel, C., Audenrieth-Kersten, I., Gahr, A., Müller, A.-L., Stracke, B., Stupar, D., Walter C., Häusler B., Remus S., Selle, J., Griebel, H., Eidel, W., Asmar, S., Goltz, G., Kahan, D., Barriot, J.-P., Dehant, V., Beuthe, M., Rosenblatt, P., Karatekin, Ö., Lainey, V., Tyler, G.L., Hinson, D., Simpson, R., Twicken, J., 2009. The Observations of the Mars express orbiter radio science (MARS) experiment after one year in orbit, ESA Scientific Publication, ESA-SP, SP-1291, 217–245.

Pätzold, M., Neubauer, F.M., Carone, L., Hagermann, A., Stanzel, C., Häusler, B., Remus, S., Selle, J., Hafl, D., Hinson, D., Simpson, R., Tyler, G.L., Asmar, S., Axford, W.I., Hagfors, T., Barriot, J.-P., Cerisier, J.-C., Imamura, T., Oyama, K.-I., Janle, P., Kirchengast, G., Dehant, V., 2010. MaRS: Mars Express Orbiter Radio Science., ESA Scientific Publication, ESA SP-1240, 141–163.

Rivoldini, A., Van Hoolst, T., Verhoeven, O., 2009. The interior structure of Mercury and its core sulfur content. Icarus 201 (1), 12–30, doi:10.1016/j.icarus.2008.12.020.

Rivoldini, A., Van Hoolst, T., Verhoeven, O., Mocquet, A., Dehant V., 2010. Geodetic constraints on the interior structure. submitted to Icarus.

Roosbeek, F., 2000. Analytical developments of rigid Mars nutation and tide generating potential series. Celest. Mech. Dyn. Astron. 75, 287–300.
Rosenblatt, P., Dehant, V., 2010. Mars geodesy and rotation. Research in Astronomy and Astrophysics (RAA), in press.
Sanloup, C., Jambon, A., Gillet, P., 1999. A simple chondritic model of Mars. Phys. Earth Planet. Inter. 112 (1–2), 43–54.
Smith, D.E., Zuber, M.T., Frey, H.V., Garvin, J.B., Head, J.W., Muhlerman, D.O., Pettengill, G.H., Phillips, R.J., Solomon, S.C., Zwally, H.J., Banerdt, W.B., Duxbury, T.C., 1998. Topography of the Northern Hemisphere of Mars from the Mars orbiter laser altimeter. Science 279 (5357), 1686.
Sohl, F., Spohn, T., 1997. The interior structure of Mars: Implications from SNC meteorites. J. Geophys. Res. 102 (E1), 1613–1636, doi:10.1029/96JE03419.
Spiga, A., Forget, F., 2009. A new model to simulate the Martian mesoscale and microscale atmospheric circulation: validation and first results. J. Geophys. Res. 114 (E2), E02009, doi:10.1029/2008JE003242.
Spohn, T., Acuña, M.H., Breuer, D., Golombek, M., Greeley, R., Halliday, A., Hauber, E., Jaumann, R., Sohl, F., 2001. Geophysical constraints on the evolution of Mars. Space Sci. Rev. 96 (1–4), 231–262.
Van den Acker, E., Van Hoolst, T., de Viron, O., Defraigne, P., Forget, F., Hourdin, F., Dehant, V., 2002. Influence of the winds and of the CO_2 mass exchange between the atmosphere and the polar ice caps on Mars' rotation. J. Geophys. Res. 107 (E7), doi:10.1029/2000JE001539.
Van Hoolst, T., Dehant, V., Defraigne, P., 2000a. Sensitivity of the free core nutation and the Chandler Wobble to changes in the interior structure of Mars. Phys. Earth planet. Inter. 117, 397–405.
Van Hoolst, T., Dehant, V., Defraigne, P., 2000b. Chandler Wobble and free core nutation for Mars. Planet. Space Sci. 48 (12–14), 1145–1151.
Van Hoolst, T., Dehant, V., de Viron, O., Defraigne, P., Barriot, J.-P., 2002. Degree-one displacements on Mars. Geophys. Res. Lett., doi:10.1029/2002GL014711.
Van Hoolst, T., Dehant, V., Roosbeek, F., Lognonné, P., 2003. Tidally induced surface displacements, external potential variations, and gravity variations on Mars. Icarus 161, 281–296, doi:10.1016/S0019-1035(2)00045-2.
Van Hoolst, T., 2007. The rotation of the terrestrial planets. Treatise Geophys. Planets Moons 10, 123–164, doi:10.1007/s11214-007-9202-6.
Van Thienen, P., Rivoldini, A., Van Hoolst, T., Lognonné, P., 2006. A top–down origin for Martian mantle plumes. Icarus 185 (1), 197–210, doi:10.1016/j.icarus.2006.06.008.
Van Thienen, P., Benzerara, K., Breuer, D., Gillmann, C., Labrosse, S., Lognonné, P., Spohn, T., 2007. Water, Life, and Planetary Geodynamical Evolution. In: Herring, T., Schubert, J. (Eds.), Treatise of Geophysics, invited paper, 129. Elsevier Publication, pp. 167–203, doi:10.1007/s11214-007-9149-7.
Verhoeven, O., Rivoldini, A., Vacher, P., Mocquet, A., Choblet, G., Menvielle, M., Dehant, V., Van Hoolst, T., Sleewaegen, J., Barriot, J.-P., Lognonné, P., 2005. Interior structure of terrestrial planets. I. Modeling Mars' mantle and its electromagnetic, geodetic and seismic properties. J. Geophys. Res. (Planets) 110 (E4), E04009, doi:10.1029/2004JE002271.
Yoder, C.F., Konopliv, A.S., Yuan, D.N., Standish, E.M., Folkner, W.M., 2003. Fluid core size of Mars from detection of the solar tide. Science 300 (5617), 299–303.
Yseboodt, M., Barriot, J.P., Dehant, V., 2003. Analytical modeling of the Doppler tracking between a lander and a Mars orbiter in term of rotational dynamics. J. Geophys. Res. 108 (E7), 5076, doi:2003JE002045.
Zharkov, V.N., Gudkova, T.V., 2000. Interior structure models, Fe/Si ratio and parameters of figure for Mars. Phys. Earth Planet. Inter. 117 (1), 407–420.
Zuber, M., Lemoine, F., Smith, D., Konopliv, A., Smrekar, S., Asmar, S., 2007. The Mars reconnaissance orbiter radio science gravity investigation. J. Geophys. Res. 112 (E5), doi:10.1029/2006JE002833 CiteID E05S07.